Müller-Navarra, K.; Milker, Y.; Bunzel, D.; Lindhorst, S.; Friedrich, J.; Arz, H.; Schmiedl, G.:
Evolution of a salt marsh in the southeastern North Sea region – Anthropogenic and natural forcing.
In: Estuarine, Coastal and Shelf Science. Vol. 218 (2019) 268 - 277.
First published online by Elsevier: 31.12.2018

https://dx.doi.org/10.1016/j.ecss.2018.12.022

Evolution of a salt marsh in the southeastern North Sea region – anthropogenic and natural forcing

Katharina Müller-Navarra[1], Yvonne Milker[1*], Dorothea Bunzel[1], Sebastian Lindhorst[1], Jana Friedrich[2], Helge Arz[3], and Gerhard Schmiedl[1]

[1]University of Hamburg, Center for Earth System Research and Sustainability, Institute for Geology, Bundesstrasse 55, 20146 Hamburg, Germany

[2]Helmholtz Centre Geesthacht, Institute of Coastal Research, Max-Planck-Strasse 1, 21502 Geesthacht, Germany

[3]Leibniz Institute for Baltic Sea Research, Seestrasse 15, 18119 Rostock, Germany

[*]corresponding author: yvonne.milker@uni-hamburg.de

Abstract

Salt-marsh sediments of the southeastern North Sea provide an archive to unravel the influences of coastal management and natural processes such as storm-tide deposition on salt-marsh development. We present a record of salt-marsh evolution during the past century from the Bay of Tümlau (northwestern Germany) based on fossil foraminiferal assemblages and sedimentological data. After diking the hinterland of the Bay of Tümlau in 1935 CE and commencing marsh management, the environment at the study site changed from a tidal flat to a salt marsh. Salt-marsh sediment accretion is influenced by recurrent dredging events, as indicated by layers rich in calcareous tidal-flat foraminifera, and redeposition of siliciclastic particles from the surrounding tidal flats during storm tides. The latter fostered the establishment of a typical salt-marsh foraminiferal fauna dominated by the agglutinating species *Entzia macrescens*. Storm-tide layers have a lighter sediment color and commonly a more negatively skewed grain-size distribution with variable sorting. The observed long-term

coarsening of the salt-marsh sediment likely reflects the landward progression of the vertical erosional cliff and the depletion of fine-grained sediment particles in the tidal flats under the influence of sea-level rise. Supra-tidal conditions, resulting from natural protection measures and abandonment of dredging, are indicated by the occurrence of *Balticammina pseudomacrescens* around 2001 CE. This species is adapted to only occasional submergence during storm tides. The recent increase in elevation is accompanied by establishment of high-marsh vegetation and characterized by a present height of the marsh surface 50 cm above mean high water springs. During the past sixty years, average sediment accretion rates decreased from 18 to 11 mm yr^{-1} reflecting the maturing of the salt marsh. These rates clearly outpace the recent mean sea-level rise in the southern North Sea demonstrating that the regional salt marshes are still resilient to sea-level rise.

Keywords: Salt-marsh evolution, coastal management, foraminifera, grain-size distribution, storm tides, sea level rise

1 Introduction

The southeastern North Sea region is frequently affected by storms and experienced the most and highest storm tides of the entire North Sea coast during the past centuries (Tomczak, 1952; Gerber et al., 2016). Hence, storm-tide protection management is crucial for populated regions such as the German North Sea coast, especially since the regional mean sea-level rise has a linear long-term trend of a 2.4 ± 0.1 mm yr^{-1}, as recorded by the Cuxhaven tide gauge over the period from 1871 to 2008 CE (Dangendorf et al., 2012, 2013). The impacts of tides, storm tides and waves on North Sea coasts, in a context of sea-level rise, and their importance when considering coastal defense strategies have been discussed for a long time (Grossmann, 1916; Schelling, 1952), although are still not well understood (Möller et al., 2014; Arns, 2017). In this context, it is essential to understand the function of

52 salt marshes in attenuating storm-tide energy and their long-term resilience to storm tides
53 with respect to lateral and surface erosion and sediment accretion (Möller et al., 2014;
54 Karimpour et al., 2017).

55 Storm tides (defined as water levels exceeding mean high water by at least 1.5 m; Müller-
56 Navarra et al., 2013; Gerber et al. 2016) occur during almost every winter, with on average
57 five storm tides per season (Gerber et al., 2016). Severe storm tides (water levels exceeding
58 mean high water by at least 2.5 m; Müller-Navarra et al., 2013; Gerber et al. 2016)
59 repeatedly impacted the coastal region and led to dike failures, losses of marsh areas and
60 numerous casualties. Examples include the so-called 'Grote Mandränke' in 1362 CE (Lamb,
61 1991; Meier, 2004) but also more recent events in 1962 CE and 1976 CE (Zitscher et al.,
62 1979; Gerber et al., 2016). Storm tides deposit large amounts of suspended matter onto the
63 salt-marsh surface when current velocity slows down due to friction with the vegetation cover
64 while storm waves propagate inland (Turner et al., 2006; Kirwan and Megonigal, 2013;
65 Schuerch et al., 2014; Fagherazzi, 2014; Leonardi et al., 2018). Consequently, storm tides
66 foster enhanced sediment deposition on salt marshes, and their surface may exceed mean
67 high water spring, independently from regional relative sea-level changes (Allen, 1990). This
68 stands in contrast to regular mean high tides, where sediment accretion is minor to non-
69 existent, as marsh surfaces elevate to and exceed mean high-tide level. Numerical modeling
70 indicates that in areas with a tidal range below 3 m and suspended sediment concentrations
71 <30 mg/l regular high tides may not supply the amount of material needed to outpace
72 accelerated sea-level rise (Kirwan et al., 2010). As a result, low marshes, which are
73 submerged for longer time periods during regular high waters, exhibit higher depositional
74 rates compared to high marshes (Kirwan and Megonigal, 2013). Results from a salt marsh
75 on the island of Sylt revealed that the sediment accretion rate of low marshes is proportional
76 to mean storm strength, while in high marshes it is mainly controlled by storm frequency
77 (Schuerch et al., 2012). Model results further suggest that an increase in storm frequency
78 can raise the ability of salt marshes to keep up with a sea-level rise of up to 3 mm yr^{-1} if

sediment supply is high enough (Kirwan et al., 2010; Schuerch et al., 2013) and accommodation space is available (Schuerch et al., 2018).

The grain-size spectrum of siliciclastic sediments depends on the grain sizes available during sedimentation and the hydrodynamic conditions during settling of particles and final burial by subsequently deposited material. The availability of siliciclastic particles is controlled by the sediment source and the processes of transport and sedimentation which could alter the original grain-size spectrum. Post-sedimentary alteration includes winnowing, i.e. the depletion of fines due to reworking, or enrichment of the fine fraction by subsequent filling of open pore space under lower energetic conditions. Mobilization of fine-grained material and subsequent mud enrichment in storm-tide deposits has been observed in salt-marsh sequences elsewhere (Reineck and Singh, 1975; Bartholdy, 2012).

Tidal flats and salt marshes are populated by benthic foraminifera. The different taxa exhibit a distinct vertical zonation relative to the tidal frame, and hence elevation in relation to mean sea level (Scott and Medioli, 1978, 1980). In this context, salt-marsh foraminifera provide an important tool for the reconstruction of past relative sea-level changes by using transfer functions (Guilbault et al., 1995; Horton and Edwards, 2006; Gehrels et al., 2006; Kemp et al, 2013; 2017) but can also be applied to the paleo-environmental reconstruction of salt marshes (Cearreta et al., 2013; Francescangeli et al., 2016; 2017). Foraminifera can also be used for the identification of events of sediment reworking such as storm layers in salt-marsh deposits (Scott et al., 2003; Kortekaas and Dawson, 2007). Fossil storm layers in salt marshes likely contain allochthonous calcareous foraminifera from tidal flats while the autochthonous fauna mainly comprises arenaceous taxa in salt marshes. The application of this proxy can be limited by the dissolution of calcareous tests, which occurs in many salt marshes worldwide (Jonasson and Patterson, 1992; Murray and Alve, 1999; Horton and Murray, 2006; Berkeley et al., 2007; Hawkes et al., 2010; Milker et al., 2015). Allochthonous foraminiferal tests may also be introduced on the sediment surface during dredging of ditches in managed salt marshes but this process has not been studied so far. The

distribution patterns of modern foraminifera in ditched and grazed salt marshes of the southeastern North Sea lack a clear separation between low- middle- and high-marsh faunas. Instead, the different species reflect the anthropogenic impacts and inhabit specific niches on the salt marsh, in ditches and ponds, depending on substrate, submergence frequency and pH (Müller-Navarra et al., 2016).

This study focuses on the temporal evolution of a managed salt marsh with artificial drainage system from the southeastern North Sea coastal region (Bay of Tümlau on Eiderstedt, northwestern Germany) during approximately the last century. We use the fossil foraminiferal assemblages preserved in the sediment section (TB13-1) to characterize the paleo-environment, specifically changes in the vertical elevation and reworking. In addition, grain-size data from this and adjacent sections TB17-1 and TB17-2 characterize storm-tide deposits and their role in the salt-marsh evolution of the Bay of Tümlau. Based on this, we address the following questions: (1) Which natural and anthropogenic processes controlled the salt-marsh evolution in the Bay of Tümlau during the past century; (2) what are the micropaleontological and sedimentological characteristics of dredging and storm-tide layers in the salt-marsh; and (3) what controls the vertical sediment accretion and lateral erosion of salt marshes and its resilience to sea-level rise?

2 Study area

The southeastern German North Sea coast is fringed by approximately 100 km^2 of salt marshes, of which 60 km^2 are located in the Wadden Sea National Park, and 36 km^2 are a nature reserve (Landesbetrieb für Küstenschutz, Nationalpark und Meeresschutz Schleswig-Holstein, LKN.SH, 2017). The salt marsh of the Bay of Tümlau is located on the Eiderstedt peninsula in the German Wadden Sea region (Fig. 1). Two inter- to subtidal sandy barriers fringe the bay since around 1878 CE (Hofstede, 1997). Eiderstedt peninsula itself was separated in several islands until around 1100 CE dikes were built in the hinterland of the bay to protect the region against storm tides (Meier, 2004).

The construction of groynes and management of artificial drainage systems aimed at enhancing clastic sedimentation in most salt marshes along the German North Sea coast (Stock, 2011). After the foundation of the Wadden Sea National Park in 1985 CE ditching and dredging was abandoned successively in protected areas but the patterns of (formerly) ditched salt marshes are still ubiquitous along the coast (Stock, 2011; Stock et al., 2005). In the salt marsh of the Bay of Tümlau ditches were implemented at a spacing of ~10 m and subsequently dredged every three to seven years (pers. comm. LKN.SH, 2017) for drainage and land-reclamation purposes. Repeated vegetation monitoring and mapping confirmed this development also for the Bay of Tümlau, where first patches of high marsh vegetation in the vicinity of the location of our studied section were documented in 2001 (Stock et al., 2005). Nowadays, the straight ditches are more and more filled with sediment and natural salt-marsh vegetation and dendritic drainage system are gradually returning. The modern dike prevents migration of the marsh belt further landwards. As a result, the marsh is under erosion and now bordered by a cliff towards the tidal flat.

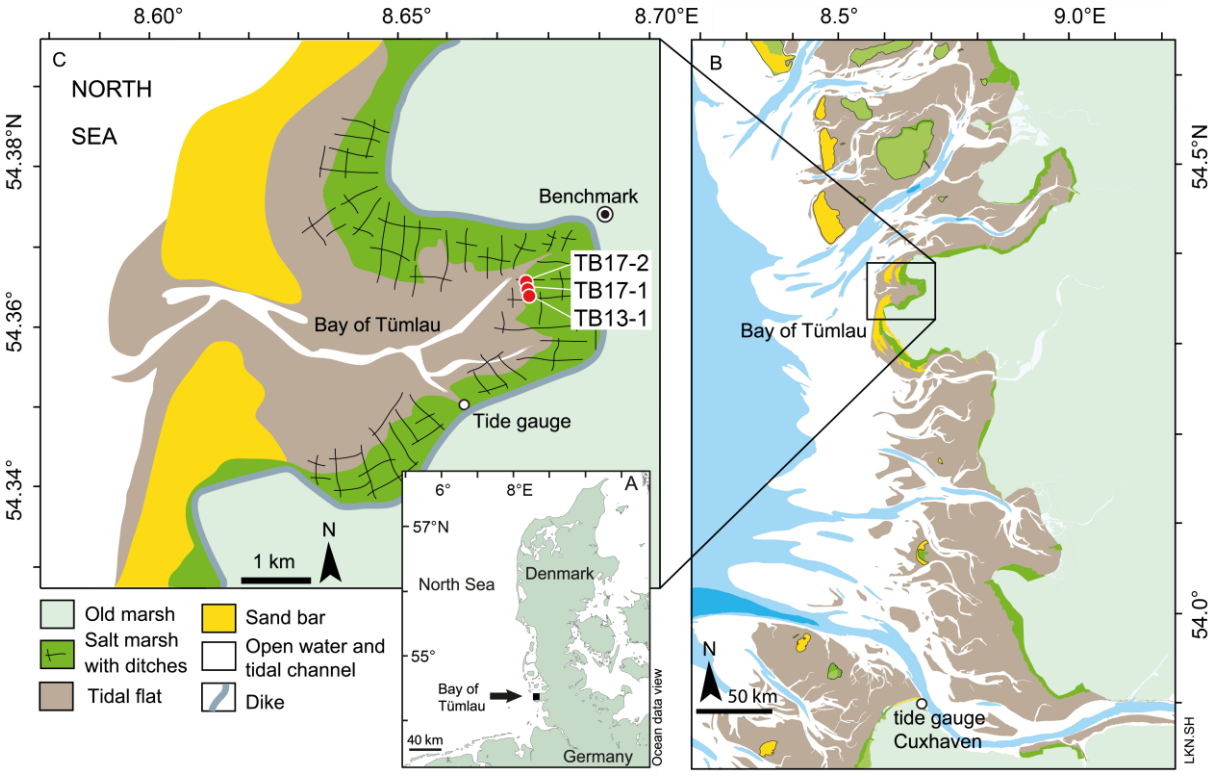

Figure 1: A) Overview of the southeastern North Sea region; B) North Frisian North Sea coast with intertidal areas and study area, and location of the tide gauge Cuxhaven; C) Bay of Tümlau on Eiderstedt peninsula with locations of study sites TB13-1, TB17-1 and TB17-2, local tide gauge and benchmark. Topographic information after Landesbetrieb für Küstenschutz, Nationalpark und Meeresschutz Schleswig-Holstein LKN.SH (2017) and Ocean Data View (Schlitzer, 2014).

Historical maps show that the study area was a tidal flat in 1919 CE, and that first salt-marsh patches were present in 1943 CE after the polder “Tümlauer Koog” was separated from the southeastern part of the Bay of Tümlau by dike construction in 1935 CE (Königlich Preussische Landes-Aufnahme, 1879 with supplement of 1919; Reichsamt für Landesaufnahme, 1943). Today, the salt marsh exhibits zones of low, middle and high marsh areas, as defined by plants although the general topography is rather flat (Fig. 2; Müller-Navarra et al., 2016). The salt-marsh vegetation close to the studied erosional cliff includes *Artemisia maritima*, *Carex extensa, Halimone portulacoides*, and *Glaux maritima*, and hence represents a high-marsh zone. The region has semi-diurnal tides, and tidal range is 1.52 m (Müller-Navarra et al., 2016). Tidal datums of the “Tümlauer Hafen” tide gauge (tide gauge number 110016, observation period: 2001-2013), installed 1.4 km away from the location of the sediment succession (Fig. 1C), include: highest astronomical tide (HAT): 2.0 m “Normalhöhennull” (NHN; German reference datum), mean high water springs (MHWS): 1.59 m NHN, mean high water (MHW): 1.44 m NHN, and mean low water (MLW): -0.07 m NHN. It should be noted that the tide gauge “Tümlauer Hafen” falls dry during low water so that the calculation of mean low water (MLW) is based on four nearby tide gauges, including Husum, Pellworm (Anleger), St. Peter Ording (Bad), and Stucklahnungshörn (observation period 2010-2015). The modern salt-marsh surface lies 0.5 cm above MHWS and no spring waters above the elevation of the marsh surface are recorded at the tide gauge “Tümlauer Hafen”, thus the salt-marsh surface is only inundated during storm tides (Fig. 2). A total of 582 storm tides were recorded at Cuxhaven tide gauge between 1843 CE and 2013 CE (data provided

by the Federal Maritime and Hydrographic Agency, BSH), 50 km south of the Bay of Tümlau (Fig. 1B).

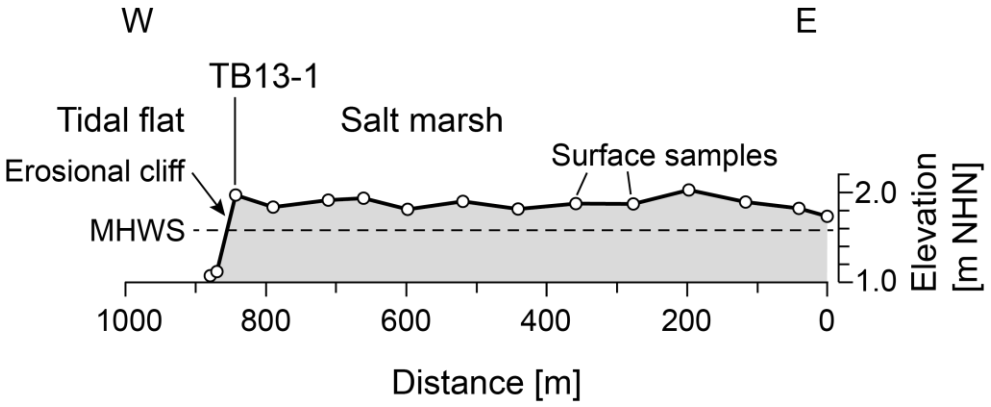

Figure 2: A) East-west surface transect F across the salt marsh in the Bay of Tümlau showing the erosional cliff, where sediment section TB13-1 was sampled (modified from Müller-Navarra et al., 2016). The dashed line marks mean high water spring (MHWS) in the Bay of Tümlau. Elevation is given in the German reference level “Normalhöhennull” (NHN).

3 Material and methods

3.1 Salt-marsh sampling

For this study, a primary sediment section (TB13-1) was sampled at an erosional cliff for foraminiferal and grain-size analysis in August 14, 2013 CE (Fig. 1C; Table 1). Two adjacent sections (TB17-1 and TB17-2) were sampled for grain-size analyses in March 17, 2017 CE (Fig 1 C; Table 1). The location and elevation of the cliff surface at sites TB13-1, TB17-1 and TB17-2 were determined with reference to a base station (trigonometric point no. 1618 031 10, Fig. 1C) by means of a Leica Geosystems AG, Viva Uno GNSS receiver, Type CS10, operated in real time kinematic mode. Raw data were processed using the software Geo Office 8.3 (Leica). Resulting uncertainty of elevations is <0.01 m. Sediment sampling was conducted using U-channels (each 120 cm long, 1.6 cm wide and 1.6 cm deep). The U-channels were pushed into the cleaned erosional face of the salt-marsh cliff and

198 subsequently detached by pulling a wire through the sediment behind the U-channels, which
199 enables the recovery of undisturbed, vertical sediment successions (Fig. 3). In the laboratory,
200 the sediment succession from site TB13-1 was described, photographed and three U-
201 channels were sliced into 1 cm aliquots, each with a volume of ~2.56 cm^3, for grain-size
202 analyses, foraminiferal investigations, and age dating, respectively. The sediment sections
203 TB17-1 and TB17-2 were sampled equidistantly (1.5 cm^3, each cm) for grain-size analyses.
204 Additionally, surface sediments along a coast normal transect (transect F; Fig. 2), deposited
205 during the winter storm flood on January 31, 2013 CE, were sampled in April 2013 CE and
206 also investigated for grain-size distribution.

207

208 Table 1: Section number, sampling date, surface height, latitude and longitude of the study
209 sites. NHN denotes the German reference level “Normalhöhennull”.

Station	Sampling date	NHN [m]	Latitude [°N]	Longitude [°E]
TB13-1	14 August 2013	2.09	54.3646	8.6775
TB17-1	17 March 2017	2.11	54.3647	8.6762
TB17-2	17 March 2017	2.19	54.3650	8.6761

210

211

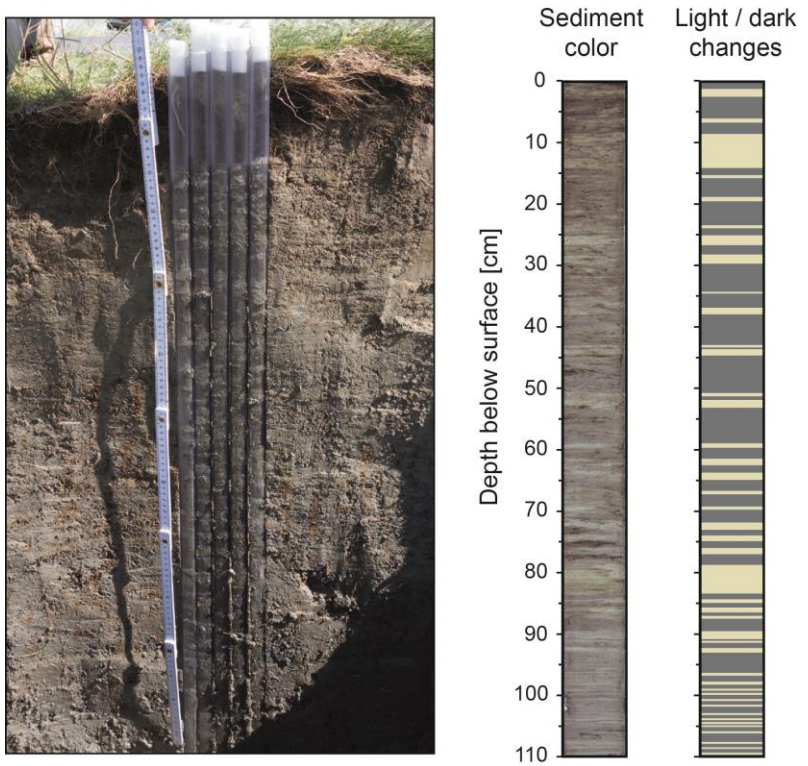

Figure 3: A) Picture of the sampling design showing five out of a total of 15 U-channels pushed into the sediment of the erosional cliff; B) Picture of section TB13-1 and generalized succession of lighter and darker layers.

3.2 Age dating

Chronologies of recent sediments up to an age of ca. 120 years can be inferred from e.g., ^{210}Pb, a natural radioactive isotope of lead, in combination with independent time markers like the artificial fallout products ^{137}Cs and ^{241}Am (Appleby, 2002). A total of 38 samples were taken from section TB13-1 to establish an age model. After determining porosity and density, and drying and grinding, the samples were closed airtight. After four weeks, sediment samples were gamma-counted for ^{210}Pb, ^{214}Bi, ^{214}Pb, ^{241}Am and ^{137}Cs on a planar broad energy GE detector (CANBERRA), and $^{210}Pb_{supported}$ (^{226}Ra) and $^{210}Pb_{unsupported}$ were calculated accordingly. $^{210}Pb_{supported}$ is constantly produced in the sediment by decay of ^{226}Ra due to authigenic material, and was calculated using the activities of the ^{226}Ra daughters ^{214}Pb and ^{214}Bi (295; 352; 609 keV lines). Subtracting $^{210}Pb_{supported}$ from the corresponding total ^{210}Pb (46.6 keV line) in each sample results in $^{210}Pb_{unsupported}$, which originates from the

atmospheric deposition (Pittauerova, 2011). The CRS (constant rate of supply) model (Appleby and Oldfield, 1978) was applied to develop the sediment chronology and to calculate mass accumulation rates (MAR) as described in detail in Appleby (2002). The CRS model assumes a constant rate of supply of $^{210}Pb_{unsupported}$ from the atmosphere. Accordingly, the $^{210}Pb_{unsupported}$ activity of the sediment varies inversely proportional to the sedimentation rate, i.e., high sediment accumulation means lower ^{210}Pb activity in the sediment due to dilution and vice versa. In order to support the ^{210}Pb-based age model, Cesium (^{137}Cs) and Americium (^{241}Am) were measured and used as independent time markers as well (Pennington et al., 1973; Hardy et al., 1973). ^{137}Cs has strongest peaks in 1963 CE, which marks the end of the atmospheric fallout from nuclear bomb testing, and in 1986 CE due to the Chernobyl accident. An additional minor peak can be probably associated with the Sellafield accident in 1957 (Ehlers et al., 1993). The ^{241}Am time marker forms by decay of ^{239}Pu, originating from fallout of atmospheric nuclear-weapons tests debris and marks the period of nuclear tests from 1952-1963 CE, with the strongest signal in 1963 CE. The distribution of errors in the measured activities is approximated by Gaussian (normal) distribution, and given as 1-sigma counting errors. The errors for sediment ages and MAR are calculated by error propagation (Binford, 1990) as the square root of the sum of the squares of the uncertainties of the individual variables, assuming normal distribution. The estimated errors in sediment ages are ±10 years and >50 years in the upper and lower parts of the section, respectively (Fig. 4).

3.3 Grain-size analyses

All samples for grain-size analysis were treated with H_2O_2 prior to measurement to oxidize the organic matter and subsequently sieved using a 2000 µm sieve to remove large plant remains. Samples were then suspended in water with addition of a 0.05-%-solution of Tetra-Sodium Diphosphate Decahydrate ($Na_4P_2O_7$ x $10H_2O$) as a dispersing agent. The particle-size distributions of the samples were determined by means of a Sympatec Helos/KF Magic

laser diffraction particle sizer (measuring range 0.5/18-3500 µm). Grain-size statistics, including mean grain size, skewness and sorting, were calculated using GRADISTAT (Blott and Pye, 2001), and are based on the graphical method (Folk and Ward, 1957).

3.4 Foraminiferal analyses

For foraminiferal analyses, 106 samples were wet sieved over 63 µm and 500 µm sieves from sediment section TB13-1. The fraction 63-500 µm was divided into equal aliquots by using a wet-splitter after Scott and Hermelin (1993) and by applying the procedure described in Gehrels (2002). Around 200 specimens per sample were counted under a stereomicroscope. The identification of foraminiferal taxa was based on Murray (1971, 1979), Gehrels and Newman (2004), and Müller-Navarra et al. (2016, 2017). Based on the census counts, the total foraminiferal density (per 10 cm^3 sediment volume) and the ratio of calcareous to agglutinated species were calculated. For quantification of reworked tidal flat foraminifera in the salt-marsh sediments a reworking index has been developed referring the relative abundance of *Elphidium excavatum* to the sum of *E. excavatum* and all agglutinated taxa (% *E. excavatum* / (% E. excavatum + % agglutinated taxa)). In the Bay of Tümlau, the modern occurrence of *Elphidium excavatum* is restricted to the tidal flats and ditches while agglutinating taxa only inhabit the salt marsh (Müller-Navarra et al., 2016).

4 Results

4.1 Sedimentology of section TB13-1

The sediments in section TB13-1 mainly consist of sandy mud. The dominant sediment color is dark-greenish gray in the lower part, which turns into a dark reddish grey in the uppermost 24 cm (Fig. 3). Intercalations of thin light greenish gray layers of variable thickness are observed throughout the section, which likely contain a lower amount of organic matter and/or less sulfides in the lower part of the section. In the lowermost part, between 110 and

96 cm depth, the section is finely laminated including frequent intercalations of lighter intervals, each with a thickness of a few mm. In the upper part of the section, the lighter layers have a higher thickness ranging from a few mm to up to 3 cm and are more unevenly spaced. Between 84 and 27 cm the sediment section contains some horizons with iron oxides as indicated by dark reddish color.

4.2 Distribution of radiogenic isotopes and age dating

The ^{137}Cs record exhibits two distinct peaks at 32 cm and 62 cm depths. The ^{137}Cs peak at 62 cm is associated with a distinctive ^{241}Am peak (Fig. 4). Below 95 cm depth, ^{137}Cs activities approach zero. The $^{210}Pb_{unsupported}$ declines quasi exponentially down to zero with depth (Fig. 4). According to its half-life of 22.6 years this indicates a sediment age of ca. 120 years at 100 cm depth. The surface sample contains very little $^{210}Pb_{unsupported}$ because of the dominance of macro-plant remains. In the upper 15 cm of the section $^{210}Pb_{unsupported}$ varies strongly between 18 and 5 $Bq \cdot kg^{-1}$ suggesting strong variability in the mass accumulation rates (Fig. 4). The $^{210}Pb_{supported}$ activity, representing the ^{210}Pb of lithogenic origin, varies between 39.5 $Bq \cdot kg^{-1}$ and 16.5 $Bq \cdot kg^{-1}$ throughout the succession. $^{210}Pb_{supported}$ represents the sedimentary background value, which is constantly produced by decay of its radioactive precursors in the lithogenic components of the sediment, and remains largely constant in steady, undisturbed environments. The variability of $^{210}Pb_{supported}$ at site TB13-1 therefore indicates variable rate of sediment supply. The estimated errors of the CRS model are ±10 years and >50 years in the upper and lower parts of the section, respectively (Fig. 4). The calculated mass accumulation rates (MAR) represent an approximation of the sedimentation rates and therefore, values for the sediment deposited prior to approximately 1950 CE are affected with high uncertainties, due to the counting errors.

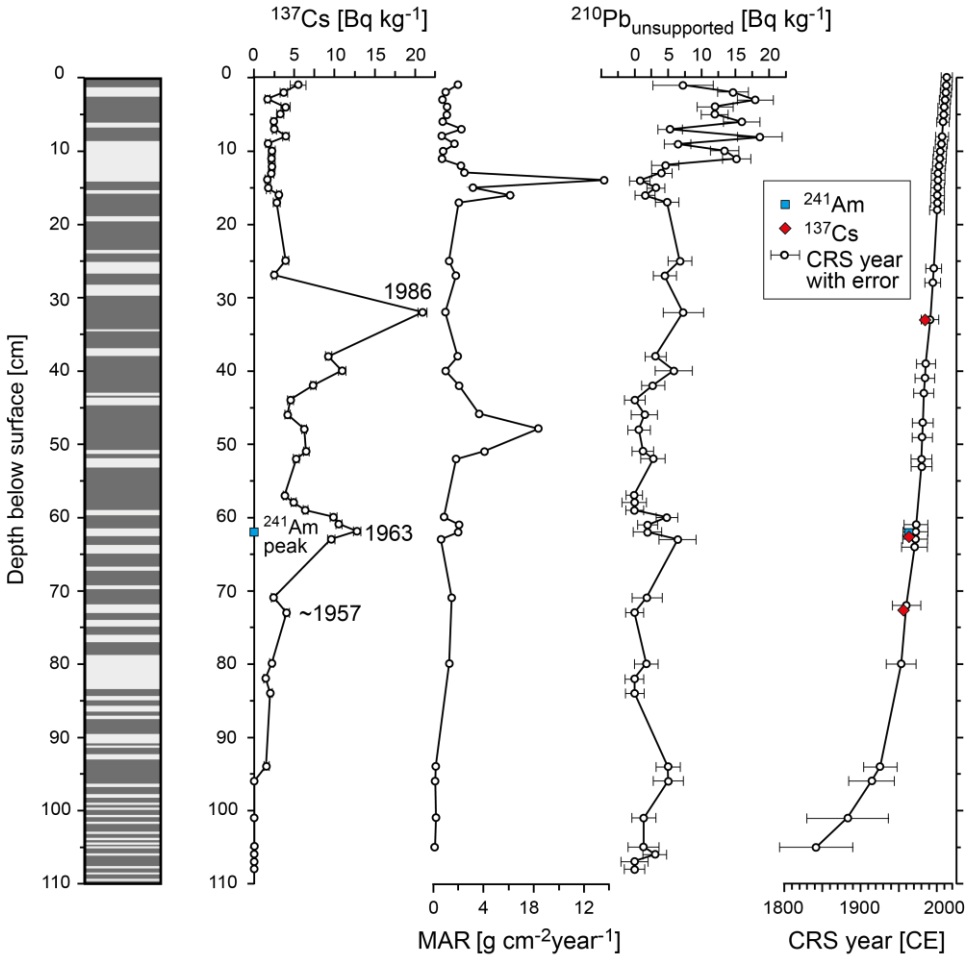

Figure 4: Age dating of the sediment succession based on ^{137}Cs, ^{241}Am, and $^{210}Pb_{unsupported}$ and derived mass accumulation rates (MAR) and results of the CRS (constant rate of supply) age model. Error bars were calculated by Gaussian error propagation and represent the 1-sigma counting error for ^{137}Cs and ^{210}Pb activities.

4.3 Grain-size distribution

The mean grain size of samples from sections TB13-1, TB17-1 and TB17-2 varies between 16.6 and 95.3 µm. The grain-size distribution is symmetrical to very fine skewed and sediments are moderately well to very poorly sorted (Fig. 5, Suppl. Fig. 1). All sections show an overall coarsening towards the sediment surface accompanied by a trend towards fewer occurrences of samples with a strongly negative skewed grain-size distribution. The mean grain size of all samples is rather controlled by the fine fraction ($r_{mean/d10}$ = 0.93; ρ < 0.00001) than by the coarse end of the grain size spectrum ($r_{mean/d90}$ = 0.75; ρ < 0.00001).

Furthermore, there is a good correlation between skewness and sorting ($r_{skewness/sorting}$ = 0.92; ρ = < 0.00001), with more negatively skewed samples being less sorted and, in general, finer-grained (Suppl. Fig. 1). The mean grain sizes of surface samples from transect F range from 8.3 to 76 µm (with 13 samples out of 16 having a mean grain size below 25 µm) (Suppl. Fig. 1). Sorting is poorly to very poorly and the grain-size distribution is very fine skewed.

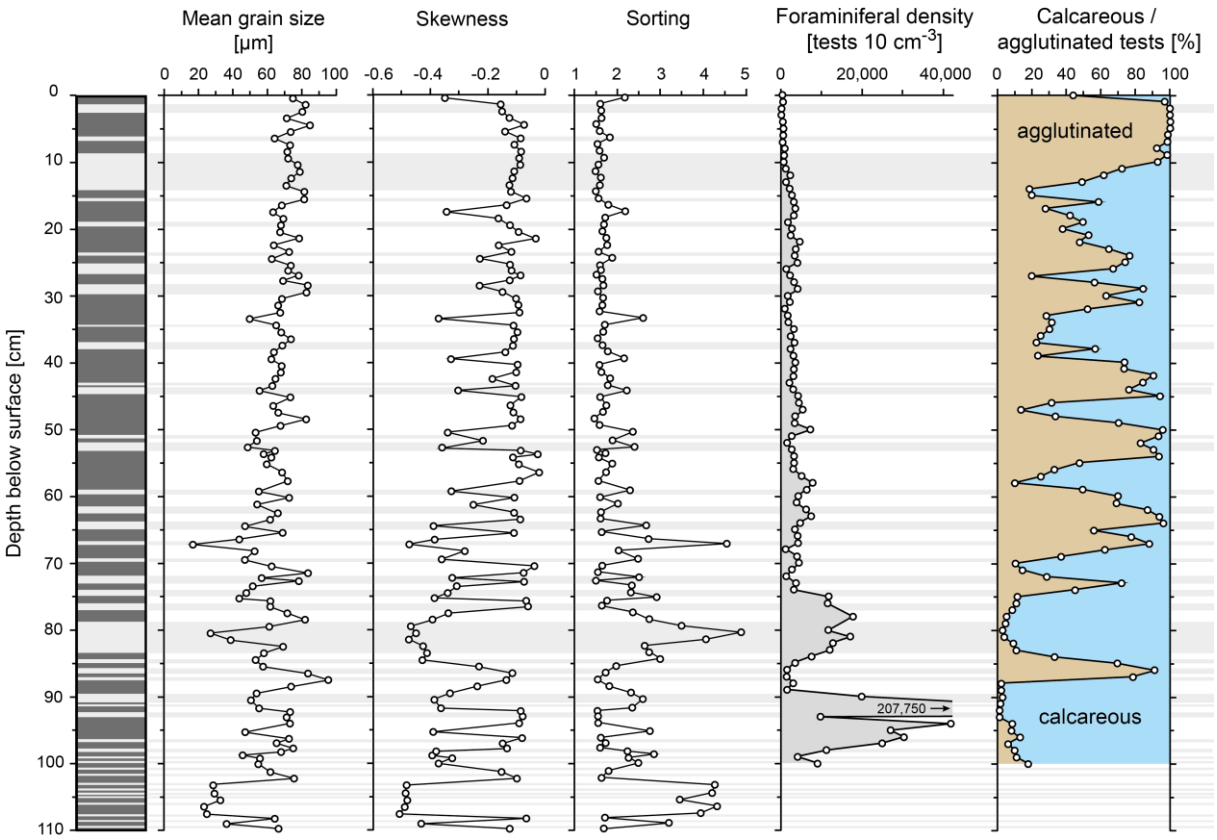

Figure 5: Mean grain size, skewness, sorting, total foraminiferal density, and ratio of calcareous and agglutinated taxa in TB13-1 versus depth. The succession of lighter and darker layers is shown for comparison.

4.4 Distribution of fossil foraminifera

A total of 24 foraminiferal taxa were identified. The most common species comprise *Entzia macrescens*, *Balticammina pseudomacrescens, Elphidium excavatum, Haynesina germanica, Ammonia batava, Trochammina inflata,* and *Elphidium williamsoni* (Fig. 6). Total foraminiferal densities are higher in the lower part of the sediment section (between 106 and

74 cm depth) with, on average, ~18,500 individuals per 10 cm^3 sediment volume and lower in the upper part of the section (between 74 and 0 cm depth) with, on average, ~3000 individuals per 10 cm^3 (Fig. 5)

The lower part of the section, between 106 and 74 cm depth, is mainly dominated by calcareous taxa, comprising *E. excavatum* (up to 80%), *H. germanica* (up to 50%), and *A. batava* (up to 20%). One exception is the interval between 87 and 84 cm depth where *E. macrescens* is the most dominant species with a relative abundance between 31 and 88%. In the middle and upper parts, between 74 and 10 cm depth, the fauna is alternately dominated by agglutinated (mainly *E. macrescens*) and calcareous taxa (mainly *E. excavatum*, *H. germanica* and *A. batava*). These alternations are also reflected in the reworking index, with a series of six pronounced maxima in this interval (Fig. 7). In the uppermost part of the section, the most abundant species are *B. pseudomacrescens* (with up to 70%), *E. macrescens* (with up to 50%) and *T. inflata* (with up to 10%) (Fig. 6).

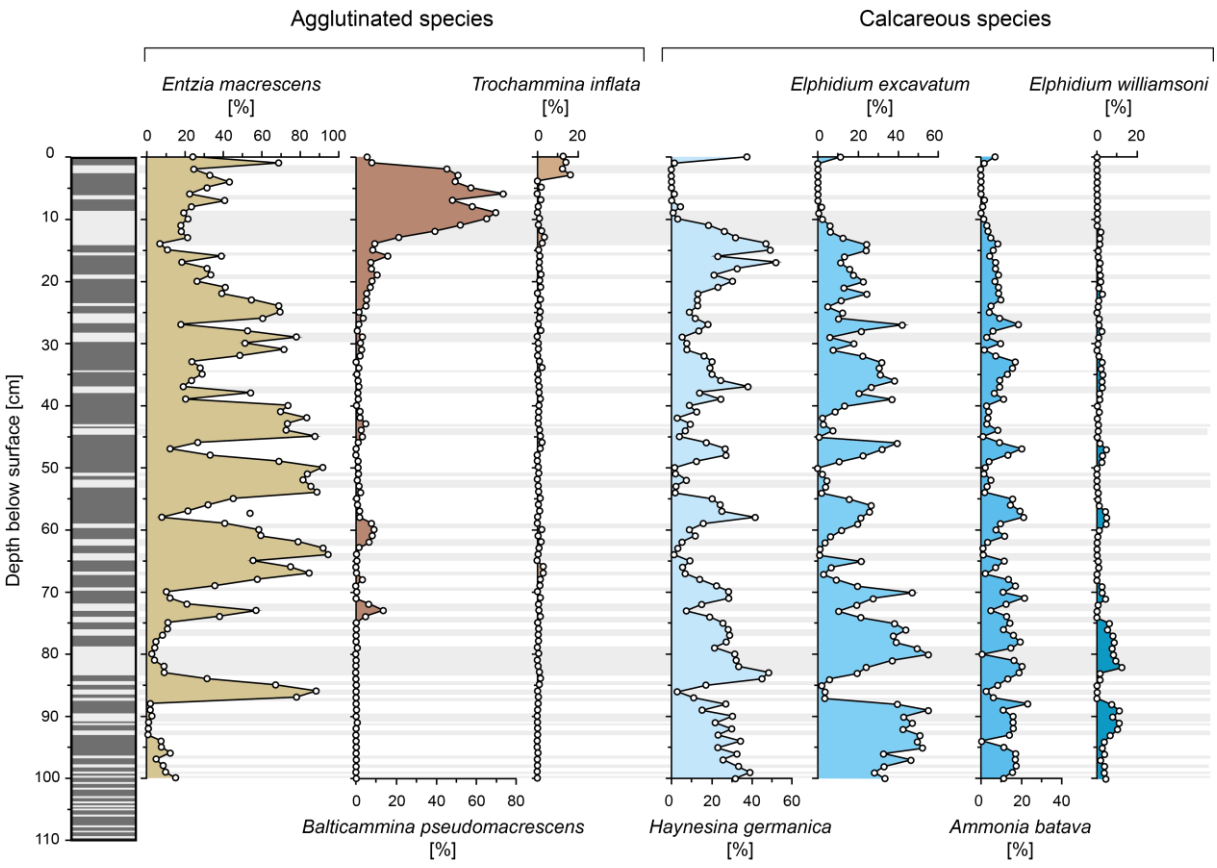

Figure 6: Relative abundance of most abundant foraminiferal species in sediment succession TB13-1 versus depth. The succession of lighter and darker layers is shown for comparison.

5 Discussion

5.1 Age model

The ^{137}Cs record exhibits two distinct peaks and implies the absence of substantial bioturbation and vertical erosion. The lower ^{137}Cs peak at 62 cm depth is associated with a distinctive ^{241}Am peak and can be related to the time of highest fallout of ^{137}Cs and ^{241}Am prior to the banning of nuclear bomb testing in 1963 CE (Delaune et al., 1978; Appleby et al. 1991; Ehlers et al., 1993). Although^{137}Cs is more mobile in the sediment (Abril, 2004) its close correspondence with the immobile ^{241}Am (Appleby et al., 1991) confirms its applicability as a reliable age marker in TB13-1. The upper ^{137}Cs peak at 33 cm depth most likely originates from the Chernobyl reactor accident in 1986 CE (Ehlers et al., 1993). Comparison with ^{137}Cs records from salt marshes of the island of Sylt suggest a relation of a minor ^{137}Cs peak at 73 cm depth with the Sellafield fire accident in 1957 CE (Ehlers et al., 1993), although this peak may be masked by the global increase in baseline values since 1954 CE (Delaune et al., 1978).

The age model based on $^{210}Pb_{unsupported}$ deviates by five to seven years from the age indicated by the ^{137}Cs and ^{241}Am markers (Fig. 4). The average atmospheric deposition of ^{210}Pb in the North Sea is 42 $Bq \cdot m^{-2} y^{-1}$, with a total flux into the sediment of 150 $Bq \cdot m^{-2} y^{-1}$ (Beks, 1997). The measured annual average lead flux in the TB13-1 is 141.1 $Bq \cdot m^{2} y^{-1}$, which is in good agreement with the literature value. The MAR show two major peaks at 15 cm and 49 cm depth with 13.5 and 8.3 g cm^{-2} $year^{-1}$, respectively, where the $^{210}Pb_{unsupported}$ activities are very low (Fig. 4). This consequently indicates dilution of the atmospheric ^{210}Pb signal by large amounts of deposited material. An alternative interpretation is the redeposition of old material (>120 years) that contains no $^{210}Pb_{unsupported}$ delivered during storm tides. Similar

377 $^{210}Pb_{unsupported}$ anomalies were observed in a Danish salt marsh and assigned to storm tides
378 (Andersen et al., 2011).

379 Due to the substantial uncertainties of the ^{210}Pb based CRS model, particularly in the lower
380 part of the section, we base our age model of TB13-1 primarily on the more reliable ^{137}Cs
381 and ^{241}Am marker horizons. An additional age control point is available with the onset of
382 high-marsh conditions at 13 cm depth, corresponding to the documented year of 2001 CE
383 (Stock et al., 2015). Within the given CRS error ranges, all age marker horizons show a good
384 agreement with the ^{210}Pb-based age model (Fig. 4).

385

386 **5.2 Salt marsh evolution in the Bay of Tümlau**

387 The sedimentary record of coastal evolution in the Bay of Tümlau preserved at site TB13-1
388 covers approximately the last 120 years with an accurate temporal frame work for the past
389 ~60 years (Figs. 4). The general salt-marsh evolution during the 20th century is accompanied
390 by coastal protection measures, including the construction of the landward dike in 1935 CE,
391 and subsequent ditching and dredging of the seaward salt marsh. The foraminiferal
392 assemblages in TB13-1 document three main periods in the evolution of the salt marsh (Fig.
393 7).

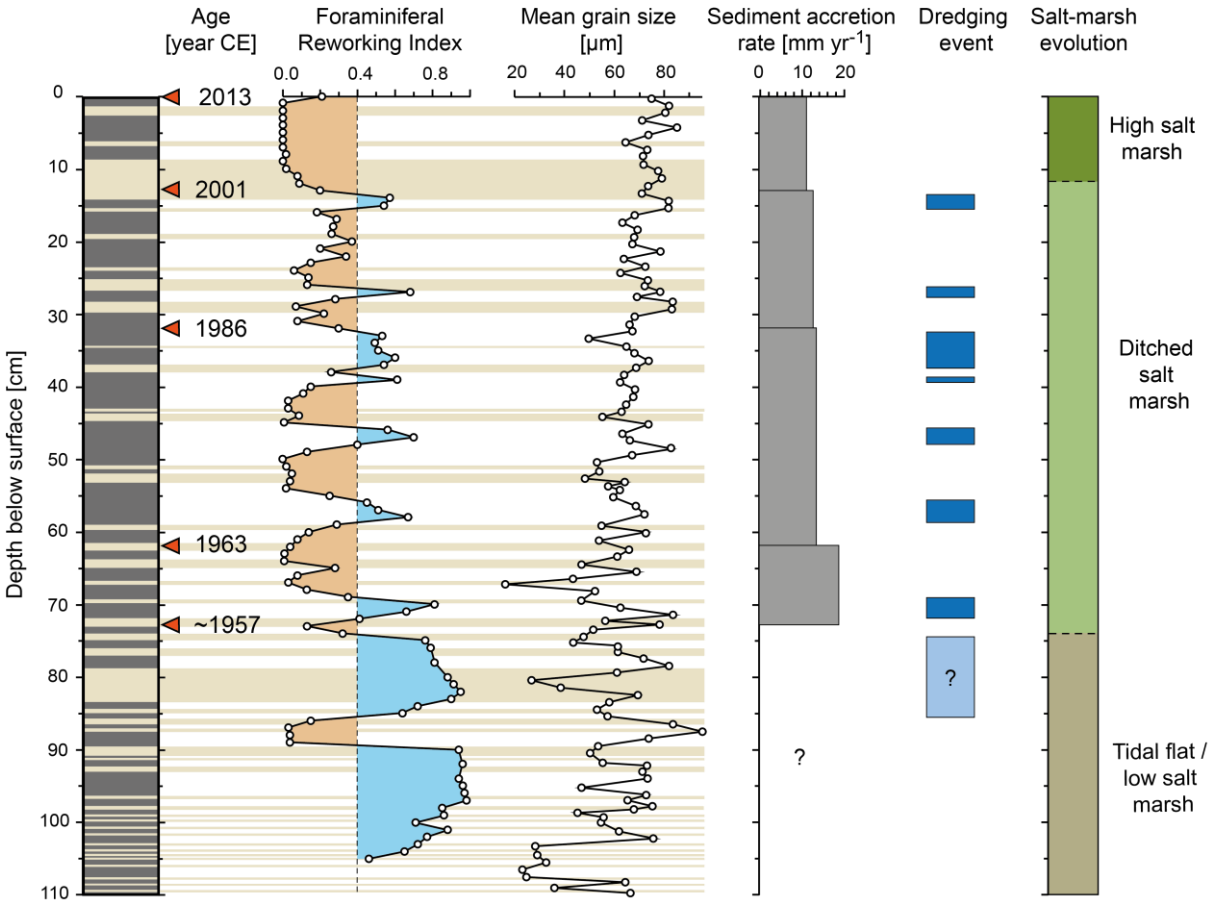

Figure 7: Comparison of the foraminiferal reworking index, mean grain size and average sediment accretion rate of TB13-1, and derived dredging events and salt-marsh evolution of the Bay of Tümlau. The succession of lighter and darker layers and reliable ages are indicated.

The first period, from the beginning of the record until the completion of the landward dike in 1935 CE and subsequent initial reclamation measures, is not constrained very well by our age model but likely includes the interval below ~75 cm depth. This sediment interval is dominated by calcareous foraminiferal tests. Dominant taxa comprise *A. batava*, *E. excavatum* and *H. germanica,* which represent characteristic species of modern tidal-flat and shallow sub-tidal environments (Francescangeli et al., 2017) and are also very common in the modern tidal flats of the Bay of Tümlau (Müller-Navarra et al., 2016). This interpretation is further supported by extremely high values of foraminiferal density (partly exceeding 20,000 tests per 10 cm^3), while densities in the shallower intervals are considerable lower (Fig. 5). A similar contrast of foraminiferal numbers between tidal flat and salt-marsh environments has

been also reported from other regions, e.g. from southwestern Denmark (Gehrels and Newman, 2004).

The second period, which extends between ~1957 and 2001 CE, is characterized by substantial fluctuations in the dominance of the agglutinating species *E. macrescens* and calcareous taxa (Figs. 5, 6). *Entzia macrescens* is a typical cosmopolitan salt-marsh species (Horton et al., 1999) and dominates the ditched and grazed salt marshes along the North Frisian coast and in southern Denmark (Gehrels and Newman, 2004; Müller-Navarra et al., 2016; 2017). This species is considered a generalist with a herbivore or detritivore feeding strategy and an epifaunal to deep infaunal microhabitat, often associated with decaying plant material (Murray, 2006, Murray and Alve, 2011). The foraminiferal density (on average 2000 individuals per 10 cm^3) during the second period is comparable to densities of dead foraminifera in the modern salt marsh of the Bay of Tümlau, which range between 2000 and 3000 individuals per 10 cm^3 (Müller-Navarra et al., 2016). The foraminiferal reworking index suggests repeated events of redeposition, which can be either attributed to storm tides or to dredging events (see discussion below).

The third period starts around 2001 CE, and is characterized by high abundances of *B. pseudomacrescens*, a high-marsh indicator in the German North Sea region (Gehrels and Newman, 2004; Müller-Navarra et al., 2017). This observation implies the establishment of supra-tidal conditions, which is confirmed by the occurrence of high-marsh vegetation (Stock et al., 2015) and the present marsh surface, which is located 50 cm above MHWS. Marsh sediment accretion during this period is controlled by storm-tide deposition and accumulation of decaying autochthonous remains from salt-marsh plants. The low values of the reworking index suggest negligible redeposition of allochthonous tidal flat foraminifera (Fig. 7).

5.3 Sedimentation processes and identification of storm-tide layers and dredging events in the Bay of Tümlau

436 Sections TB13-1, TB17-1 and TB17-2 and surface transect F are located inside the Bay of
437 Tümlau and are protected from larger waves by the sand bars which close the bay mouth
438 towards the open North Sea (Fig. 1B). A small fetch and shallow water depths inside the bay
439 prevent the built-up of large waves in the bay, even during storms. Sediments are therefore
440 deposited under comparable low-energy conditions and reworking of material from the active
441 marsh should be minor. This view is supported by mean grain sizes in the coarse silt to fine
442 sand range (Fig. 5, Suppl. Fig. 1).

443 Based on skewness data, samples of sections TB13-1, TB17-1 and TB17-2 are qualitatively
444 assigned to two distinct grain-size populations, termed GSP-1 and -2. Samples of GSP-1
445 cluster around a skewness of -0.1 and are moderately well sorted (around 1.5), whereas
446 samples of GSP-2 have a greater variability in sorting and are more negatively skewed
447 (lower than -0.2; Suppl. Fig. 1). GSP-2 samples, in general, have a smaller mean grain size
448 than GSP-1 samples. All samples of transect F, sampled from sediments deposited by a
449 known storm tide (Suppl. Fig. 1), belong to GSP-2. Based on this and given that differences
450 in grain-size reflect different hydrodynamic conditions during transport and sedimentation of
451 clastic particles, GSP-1 and -2 are interpreted to reflect fair-weather and storm
452 sedimentation, respectively. In addition, the dominance of symmetrical to fine skewed grain-
453 size populations and the absence of coarse skewed sediments suggests deposition during
454 suspension settling and absence of fast tidal currents at sites TB13-1, TB17-1 and TB17-2,
455 as also observed by Rahman and Plater (2014) in UK marshes. GSP-2 samples are
456 preferably associated with the relatively lighter layers in TB13-1 suggesting that these layers
457 represent storm-tide events (Fig. 5).

458 The observed enrichment of fine material in the storm layers is interpreted to reflect the
459 prolonged clastic sedimentation on the marsh due to increased water levels and increased
460 availability of fine material due to enhanced storm-wave erosion at the mud-flat area inside
461 the bay. Mobilization of fine-grained material and subsequent mud enrichment in storm
462 deposits on salt marshes are well known characteristics of salt-marsh sequences elsewhere

(Reineck and Singh, 1975; Bartholdy, 2012). Goodbred and Hine (1995), in addition, observed re-suspended near-shore sediments with variable grain-size distribution, showing a mineralogical similarity between storm-tide deposits and underlying marsh sediments. The suspension load consists of single clastic particles, sediment aggregates and flocculated material (Christiansen et al., 2000), and is subsequently transported onto the salt marsh surface where it is trapped by the vegetation (Fagherazzi et al., 2013; Brandon et al., 2014; Rahman and Plater, 2014; Chaumillon et al., 2017). In summary, the grain-size characteristics and composition of storm-tide layers in the section are controlled by the regional effects of sediment sources, i.e., erosion of tidal-flat and former salt-marsh deposits, submergence time, and vegetation cover.

According to observations in other regions (Scott et al., 2003; Kortekaas and Dawson, 2007), storm-tide deposits in salt marshes may also contain a considerable number of allochthonous tidal-flat foraminifera. The sediments of TB13-1 lack any larger shell fragments demonstrating the absence of high-energy conditions in the Bay of Tümlau during storm-tide deposition of clastic sediment corroborating the granulometric results. The foraminiferal reworking index exhibits six distinct intervals with dominance of allochthonous tests in the interval between ~1957 and 2001 CE. These layers are sharply bordered, occur roughly every seven to eight years, and do not correlate with the suspected lighter storm-tide layers, suggesting a different origin (Fig. 7). It appears most likely that these layers represent dredging events, when large amounts of sediment were redistributed from ditches onto the surface of the adjacent salt marsh leaving layers of 1-7 cm thickness in TB13-1. In comparison, the number of allochthonous tests, which were reworked during storm tides is obviously considerably lower. The largely absence of clear peaks in the reworking index in the intervals between the dredging events may also be attributed to the ability of *Entzia macrescens* to inhabit infaunal microhabitats (Murray, 2006; Berkeley et al., 2007) resulting in attenuation of the faunal signals.

5.4 Vertical salt-marsh sediment accretion, lateral erosion, and resilience to sea-level rise

Vertical salt marsh sediment accretion at site TB13-1 ranges between 18 and 13 mm yr^{-1} during the phase of dredging and grazing (~1950-2001 CE) and 11 mm yr^{-1} in recent years when the marsh has been submerged only during storm tides. The long-term decrease of sediment accretion rates reflects the commonly observed decrease of inundation frequencies with increasing elevation in mature salt marshes (Allen, 2000; Bartholdy et al., 2004). The recorded values are similar to those reported from other salt marshes of the German North Sea coast (Schuerch et al., 2012; Nolte et al., 2013) and demonstrate the potential of both ditched and natural marshes to outpace the present rate of relative sea-level rise of ~2.4 ±0.1 mm yr^{-1}, even when the effects of sediment autocompaction are considered (Allen, 2000; Bartholdy et al., 2010). Similarly, high sediment accretion rates of up to 16 mm yr^{-1} in a back-barrier salt marsh on the island of Sylt, 57 km north of the study site, are the result of increased storm frequency and intensity during the 1980s and 1990s CE (Schuerch et al., 2012). These results demonstrate the high potential of salt marshes to withstand sea-level rise as long as they are able to migrate inland (Kirwan et al., 2016).

Although storm tides deliver substantial amounts of sediment to the salt marsh, the increase of the elevation gradient between the tidal flat- and the salt-marsh surface may enhance the erosive impact of incoming storm-tide waves at the transitional face (Leonardi et al., 2018). In the Bay of Tümlau, a retreating cliff developed since the 1960s CE (LKN.SH, 2017). Aerial images and repeated vegetation monitoring suggest only minor retreat since 1988 CE (Stock et al., 2005). A similar evolution has been documented for UK salt marshes (Allen and Haslett, 2014). The feedbacks mechanisms between lateral marsh erosion and regeneration, however, are not yet fully understood.

Grain-size trends across salt-marsh platforms, leading to a proximal-to-distal fining of the sediments, are interpreted to reflect the lateral gradient in depositional energy (Schuerch et al., 2012; Leonardi et al., 2018). Consequently, the long-term coarsening of the sediment in

517 all three investigated sections in the Bay of Tümlau (Figs. 5, 7, Suppl. Fig. 1) is interpreted to
518 result mainly from the backward erosion of the cliff face, towards the locations of the studied
519 sediment sections. The establishment of the dike in 1935 CE, which borders the marsh
520 towards the land, impedes the lateral shift of intertidal facies zones under the influence of
521 sea-level rise (Flemming and Nyandwi, 1994; Dellwig et al., 2000; Doody 2004) and could
522 have further triggered a coarsening of the sediment.

523

524 **6 Conclusions**

525 Foraminiferal, sedimentological and geochemical data from a ^{137}Cs and ^{210}Pb dated salt-
526 marsh succession of the Bay of Tümlau (southeastern North Sea coast) are used to
527 reconstruct the development of a managed salt marsh, and for the identification of storm-tide
528 and dredging events. The benthic foraminiferal fauna reflects three periods of salt-marsh
529 evolution, accompanied by significant changes in elevation and environmental conditions.
530 Following a period of tidal-flat deposition, a managed salt marsh established at latest by the
531 end of the 1950s CE. Until 2001 CE, the salt-marsh fauna is dominated by the generalist
532 *Entzia macrescens*, which characterizes the ditched salt marshes in the entire southeastern
533 North Sea region. The dredging of ditches, which occurred approximately every seven to
534 eight years, is documented by sharply confined intervals of variable thickness, which are
535 dominated by allochthonous calcareous tidal-flat species (particularly *Elphidium excavatum,*
536 *Haynesina germanica*, and *Ammonia batava*). After protection of the salt marsh and
537 abandonment of dredging and gracing, supratidal conditions established, accompanied by
538 the occurrence of the high marsh indicator *Balticammina pseudomacrescens*. Within the
539 sediment succession, relatively lighter coarse silt to fine sand layers with strongly negative
540 skewness and variable sorting suggest deposition during storm tides but under relatively low
541 energy conditions in the Bay of Tümlau. The lack of strong waves within the bay is also
542 confirmed by the absence of shell layers and the minor amount of allochthonous tidal-flat
543 foraminifera apart from the dredging layers. The long-term coarsening of the salt-marsh

sediments likely reflects the lateral progression of the salt-marsh cliff and the gradual depletion of fine-grained sediments in the source area of the mud flats. Since ~1957 CE sediment accretion rates decreased from approximately 18 to 11 mm yr^{-1} reflecting the maturing of the salt marsh. These accretion rates are comparable to those measured in other salt marshes of the region and they outpace the relative sea-level rise of ~2.4 ±0.1 mm yr^{-1}, demonstrating the potentially high resilience of both managed and natural salt marshes to sea-level rise.

ACKNOWLEDGEMENTS

We acknowledge H.-D. Martens (LKN.SH) for providing detailed insights into anthropogenic influences on the Bay of Tümlau. S. Müller-Navarra and colleagues (BSH) provided tidal data and calculated water-level differences. We thank J. Richarz for grain-size analyses and M. Paul, M. Theodor, and H. A. Winkelbauer for support in the field and laboratory. We also thank R. Barnett and two anonymous colleagues for constructive reviews. This work was supported by the Deutsche Forschungsgemeinschaft (DFG) as part of the Center of Excellence “Climate System Science and Prediction (CliSAP)” and the Special Priority Program SPP 1889 “Regional Sea Level Change and Society” (grant SCHM1180/19). The raw data to this article will be stored at the PANGAEA data base.

REFERENCES

Abril, J.M., 2004. Constraints on the use of ^{137}Cs as a time-marker to support CRS and SIT chronologies. Environmental Pollution, 129, 31-37.

Allen, J.R.L., 2000. Morphodynamics of Holocene salt marshes: a review sketch from the Atlantic and Southern North Sea coasts of Europe. Quaternary Science Reviews, 19, 1155-1231.

569 Allen, J.R.L., Haslett, S.K., 2014. Salt-marsh evolution at Northwick and Aust warths, Severn
570 Estuary, UK: a case of constrained autocyclicity. Atlantic Geology, 50, 1-17.
571 Andersen, T.J., Svinth, S., Pejrup, M., 2011. Temporal variation of accumulation rates on a
572 natural salt marsh in the 20th century - The impact of sea level rise and increased
573 inundation frequency. Marine Geology, 279, 178-187.
574 Appleby, P.G., 2002. Chronostratigraphic techniques in Recent sediments. In: Last, W.M.,
575 Smol, J.P. (Eds.), Tracking environmental change using lake sediments.
576 Developments in Paleoenvironmental Research, 1, Springer, Dordrecht, 171-203.
577 Appleby, P. G., Oldfield, F., 1978. The calculation of Lead-210 dates assuming a constant
578 rate of supply of unsupported 210Pb to the sediment. Catena, 5, 1-8.
579 Appleby, P.G., Richardson, N., Nolan, P.J., 1991. ^{241}Am dating of lake sediments.
580 Hydrobiologia, 214, 35-42.
581 Arns, A., Dangendorf, S., Jensen, J., Talke, S., Bender, J., Pattiaratchi, C., 2017. Sea-level
582 rise induced amplification of coastal protection design heights. Scientific Reports, 7,
583 40171, doi:10.1038/srep40171.
584 Bartholdy J., 2012. Salt Marsh Sedimentation. In: Davis Jr. R., Dalrymple R. (Eds.),
585 Principles of tidal sedimentology. Springer, Dordrecht, 151-185.
586 Bartholdy, J., Christiansen, C., Kunzendorf, H., 2004. Long term variations in backbarrier salt
587 marsh deposition on the Skallingen peninsula - the Danish Wadden Sea. Marine
588 Geology, 203, 1-21.
589 Bartholdy, J., Pedersen, J.B.T., Bartholdy, A.T., 2010. Autocompaction of shallow silty salt
590 marsh clay. Sedimentary Geology, 223, 310-319.
591 Beks, J.P., 1997. The ^{210}Pb budget of the North Sea. Atmospheric input versus sediment
592 flux. In: Germain, P., Guary, J.C., Guegueniat, P., Metivier, H. (Eds.), RADOC 96-97,
593 Radionuclides in the Oceans, Cherbourg-Octeville, 219-224.
594 Berkeley, A., Perry, C.T., Smithers, S.G., Horton, B.P., Taylor, K.G., 2007. A review of the
595 ecological and taphonomic controls on foraminiferal assemblage development in
596 intertidal environments. Earth-Science Reviews, 83, 205-230.

597 Binford, M.W., 1990. Calculation and uncertainty analysis of ^{210}Pb dates for PIRLA project
598 lake sediment cores. Journal of Paleolimnology, 3, 253-267.
599 Blott, S.J., Pye, K., 2001. GRADISTAT: a grain size distribution and statistics package for the
600 analysis of unconsolidated sediments. Earth Surface Processes and Landforms, 26,
601 1237-1248.
602 Brandon, C.M., Woodruff, J.D., Donnelly, J. P., Sullivan, R. M., 2014. How unique was
603 hurricane Sandy? Sedimentary reconstructions of extreme flooding from New York
604 harbor. Scientific Reports, 4, 7366, doi:10.1038/srep07366.
605 Cearreta, A., García-Artola, A., Leorri, E., Irabien, M.J., Masque, P., 2013. Recent
606 environmental evolution of regenerated salt marshes in the southern Bay of Biscay:
607 Anthropogenic evidences in their sedimentary record. Journal of Marine Systems,
608 109-110, S203-S212.
609 Chaumillon, E., Bertin, X., Fortunato, A. B., Bajo, M., Schneider, J. L., Dezileau, L., Walsh, J.
610 P., Michelot, A., Chauveau, E., Creach, A., Henaff, A., Sauzeau, T., Waeles, B.,
611 Gervais, B., Jan, G., Baumann, J., Breilh, J. F., Pedreros, R., 2017. Storm-induced
612 marine flooding: Lessons from a multidisciplinary approach. Earth-Science Reviews,
613 165, 151-184.
614 Christiansen, T., Wiberg, P.L., Milligan, T.G., 2000. Flow and sediment transport on a tidal
615 salt marsh surface. Estuarine Coastal and Shelf Science, 50, 315-331.
616 Dangendorf, S., Wahl, T., Hein, H., Jensen, J., Mai, S., Mudersbach, C., 2012. Mean sea
617 level variability and influence of the North Atlantic Oscillation on long-term trends in
618 the German Bight. Water, 4, 170-195.
619 Dangendorf, S., Wahl, T., Nilson, E., Klein, B., Jensen, J., 2013. Characteristics of intra-,
620 inter-annual and decadal sea-level variability and the role of meteorological forcing:
621 the long record of Cuxhaven. Ocean Dynamics, 63, 209-224.
622 Delaune, R.D., Patrick Jr., W.H., Buresh, R.J., 1978. Sedimentation rates determined by
623 ^{137}Cs dating in a rapidly accreting salt marsh. Nature, 275, 532-533.

624 Dellwig, O., Hinrichs, J., Hild, A., Brumsack, H.-J., 2000. Changing sedimentation in tidal flat
625 sediments of the southern North Sea from the Holocene to the present: a
626 geochemical approach. Journal of Sea Research, 44, 195-208.
627 Doody, J.P., 2004. 'Coastal squeeze' – an historical perspective. Journal of Coastal
628 Conservation, 10, 129-138.
629 Ehlers, J., Nagorny, K., Schmidt, P., Stieve, B., Zietlow, K., 1993. Storm surge deposits in
630 North Sea salt marshes dated by ^{134}Cs and ^{137}Cs determination. Journal of Coastal
631 Research, 9, 698-701.
632 Fagherazzi, S., Wiberg, P.L., Temmerman, S., Struyf, E., Zhao, Y., Raymond, P.A., 2013.
633 Fluxes of water, sediments, and biogeochemical compounds in salt marshes.
634 Ecological Processes, 3, 1-16.
635 Fagherazzi, S., 2014. Coastal processes: Storm-proofing with marshes. Nature Geoscience,
636 7, 701-702.
637 Flemming, B.W., Nyandwi, N., 1994. Land reclamation as a cause of fine-grained sediment
638 depletion in backbarrier tidal flats (Southern North Sea). Netherlands Journal of
639 Aquatic Ecology, 28, 299-307.
640 Folk, R.L., Ward, W.C., 1957. Brazos River bar: a study in the significance of grain size
641 parameters. Journal of Sedimentary Petrology, 27, 3-26.
642 Francescangeli, F., Armynot du Chatelet, E., Billon, G., Trentesaux, A., & Bouchet, V.M.P.,
643 2016. Palaeo-ecological quality status based on foraminifera of Boulogne- sur-Mer
644 harbour (Pas-de-Calais, Northeastern France) over the last 200 years. Marine
645 Environmental Research, 117, 32-43.
646 Francescangeli, F., Bouchet V.M.P., Trentesaux A., Armynot du Chatelet E., 2017. Does
647 elevation matter? Living foraminiferal distribution in a hyper tidal salt marsh (Canche
648 Estuary, Northern France). Estuarine, Coastal and Shelf Science, 194, 192-204.
649 Gehrels, W.A., 2000, Using foraminiferal transfer functions to produce high-resolution sea-
650 level records from salt-marsh depos- its, Maine, USA. The Holocene, 10, 367-376.

651 Gehrels, W.R., Newman, S.W.G., 2004. Salt-marsh foraminifera in Ho Bugt, western
652 Denmark, and their use as sea-level indicators. Geografisk Tidsskrift, Danish Journal
653 of Geography, 104, 97-106.
654 Gehrels, W.R., Marshall, W.A., Gehrels, M.J., Larsen, G., Kirby, J.R., Eiríksson, J.,
655 Heinemeier, J., Shimmield, T., 2006. Rapid sea-level rise in the North Atlantic Ocean
656 since the first half of the nineteenth century: The Holocene, 16, 949-965.
657 Gerber, M., Ganske, A., Müller-Navarra, S., Rosenhagen, G., 2016. Categorisation of
658 meteorological conditions for storm tide episodes in the German Bight.
659 Meteorologische Zeitschrift, 25, 447-462.
660 Goodbred, S.L., Hine, A.C., 1995. Coastal storm deposition: saltmarsh response to a severe
661 extratropical storm, March 1993, west-central Florida. Geology, 23, 679-682.
662 Grossmann, L.A. 1916. Die Sturmfluten an der Deutschen Nordseeküste am 13. Januar und
663 16./17. Februar 1916. Annalen der Hydrographie, 44, 361-380.
664 Guilbault, J.-P., Clague, J.J., Lapointe, M., 1995. Amount of subsidence during a late
665 Holocene earthquake - evidence from fossil tidal marsh foraminifera at Vancouver
666 Island, west coast of Canada: Palaeogeography, Palaeoclimatology, Palaeoecology,
667 118, 49-71.
668 Hardy, E. P., Krey, P. W., Volchok, H. L., 1973. Global inventory and distribution of fallout
669 plutonium. Nature, 241, 444-445.
670 Hawkes, A.D., Horton, B.P., Nelson, A.R., Hill, D.F., 2010. The application of intertidal
671 foraminifera to reconstruct coastal subsidence during the giant Cascadia earthquake
672 of AD 1700 in Oregon, USA. Quaternary International, 122, 116-140.
673 Hofstede, J.L.A., 1997. Morphologie des St. Peter-Ording-Sandes. Die Küste, 59, 143-172.
674 Horton, B.P., Edwards, R.J., Lloyd, J. M., 1999. A foraminiferal-based transfer function:
675 Implications for sea-level studies. Journal of Foraminiferal Research, 29, 117-129.
676 Horton, B.P., Edwards, R.J., 2006. Quantifying Holocene sea-level change using intertidal
677 Foraminifera: Lessons from the British Isles. Cushman Foundation for Foraminiferal
678 Research, Special Publication, 40, 1-97.

679 Horton, B.P., Murray, J.W., 2006. Patterns in cummulative increase in live and dead species
680 from foraminiferal time serie of Cowpen Marsh, Tees Estuary, UK: Implications for
681 sea-level studies. Marine Micropaleontology, 58, 287-315.
682 Jonasson, K.E., Patterson, R.T., 1992. Preservation potential of salt marsh foraminifera from
683 the Fraser River delta, British Columbia. Micropaleontology, 38, 289-301.
684 Karimpour, A., Chen, Q., Twilley, R.R., 2017. Wind wave behavior in fetch and depth limited
685 estuaries. Scientific Reports, 7, 40654. doi:10.1038/srep40654.
686 Kemp, A.C., Horton, B.P., Vane, C.H., Bernhardt, C. E., Corbett, D. R., Engelhart, S. E
687 Anisfeld, S.C., Parnell, A.C., Cahili, N., 2013. Sea-level change during the last 2500
688 years in New Jersey, USA. Quaternary Science Reviews, 81, 90-104.
689 Kemp, A.C., Kegel, J.J., Culver, S.J., Barber, D.C., Mallinson, D.J., Leorri, E., Bernhardt,
690 C.E., Cahill, N., Riggs, S.R., Woodson, A.L., Mulligan, R.P., Horton, B.P., 2017.
691 Extended late Holocene relative sea-level histories for North Carolina, USA.
692 Quaternary Science Reviews, 160, 13-30.
693 Kirwan, M.L., Guntenspergen, G.R., D'Alpaos, A., Morris, M.T., Mudd, S.M., Temmerman, S.,
694 2010. Limits on the adaptability of coastal marshes to rising sea level. Geophysical
695 Research Letters, 37, L23401, doi:23410.21029/22010GL045489.
696 Kirwan, M.L., Megonigal, P., 2013. Tidal wetland stability in the face of human impacts and
697 sea-level rise. Nature, 504, 53-60.
698 Kirwan, M.L., Temmerman, S., Skeehan, E.E., Guntenspergen, G.R., Fagherazzi, S., 2016.
699 Overestimation of marsh vulnerability to sea level rise, Nature Climate Change, 6,
700 253-260.
701 Königlich Preussische Landes-Aufnahme, 1879. Nachträge 1919. Topographische Karte
702 1:25,000, Blatt:1618, Garding.
703 Kortekaas, S., Dawson, A.G., 2007. Distinguishing tsunami and storm deposits: An example
704 from Martinhal, SW Portugal. Sedimentary Geology, 200, 208-221.
705 Lamb, H., 1991. Historic storms of the North Sea, British Isles and Northwest Europe.
706 Cambridge University Press, Cambridge, 228 pp.

Leonardi, N., Carnacina, I., Donatelli, C., Ganju, N.K., Plater, A.J., Schürch, M., Temmerman, S., 2018. Dynamic interactions between coastal storms and salt marshes: A review. Geomorphology, 301, 92-107.

LKN.SH, 2017. Landesbetrieb für Küstenschutz, Nationalpark und Meeresschutz Schleswig-Holstein. http://www.schleswig-holstein.de/DE/Landesregierung/LKN/lkn_node.html.

Meier, D., 2004. Man and environment in the marsh area of Schleswig–Holstein from Roman until late Medieval times. Quaternary International, 112, 55-69.

Milker, Y., Horton, B.P., Nelson, A.R., Engelhart, S.E., Witter, R.C., 2015. Variability of intertidal foraminiferal assemblages in a salt marsh, Oregon, USA. Marine Micropaleontology, 118, 1-16.

Möller, I., Kudella, M., Rupprecht, F., Spencer, T., Paul, M., van Wesenbeeck, B.K., Wolters, G., Jensen, K., Bouma, T.J., Miranda-Lange, M., Schimmels, S., 2014. Wave attenuation over coastal salt marshes under storm surge conditions. Nature Geoscience, 7, 727-731.

Müller-Navarra, K., Milker, Y., Schmiedl, G., 2016. Natural and anthropogenic influence on the distribution of salt marsh foraminifera in the Bay of Tümlau, German North Sea. Journal of Foraminiferal Research, 46, 61-74.

Müller-Navarra, K., Milker, Y., Schmiedl, G., 2017. Applicability of transfer functions for relative sea-level reconstructions in the southern North Sea coastal region based on salt-marsh foraminifera. Marine Micropaleontology, 135, 15-31.

Müller-Navarra, S., Jensen, J., Rosenhagen, G., Dangendorf, S., 2013. Rekonstruktion von Gezeiten und Windstau am Pagel Cuxhaven 1843 bis 2013. Annalen der Meteorologie, 46, 50-56.

Murray, J.W., 1971. An Atlas of British Recent Foraminiferids: Heinemann Educational Books, London, 244 pp.

Murray, 1979. British nearshore foraminiferids. In: Kermack, D. M., Barnes, R. S. K., (Eds.), Synopses of the British Fauna (New Series), no. 16: Academic Press, London, 62 pp.

734 Murray, J.W., 2006. Ecology and Applications of Benthic Foraminifera. Cambridge:
735 Cambridge University Press. 426 pp.
736 Murray, J.W., Alve, E., 1999. Natural dissolution of modern shallow water benthic
737 foraminifera: taphonomic effects on the palaeoecological record. Palaeogeography,
738 Palaeoclimatology, Palaeoecology, 146, 195-209.
739 Murray, J.W., Alve, E., 2011. The distribution of agglutinated foraminifera in NW European
740 seas: Baseline data for the interpretation of fossil assemblages. Palaeontologia
741 Electronica, 14(2), 14A, 1-41.
742 Nolte, S., Müller, F., Schuerch, M., Wanner, A., Esselink, P., Bakker, J.P., Jensen, K., 2013.
743 Does livestock grazing affect sediment deposition and accretion rates in salt
744 marshes? Estuarine, Coastal and Shelf Science, 135, 296-305.
745 Pennington, W., Cambray, R.S., Fisher, E.M., 1973. Observations on lake sediments using
746 fallout Cs-137 as a Tracer. Nature, 242, 324-326.
747 Pittauerová, D., Hettwig, B., Fischer, H.W., 2012. Pb-210 sediment chronology: Focused on
748 supported lead. Radioprotection, 46, S277-S282.
749 Rahman, R., Plater, A.J., 2014. Particle-size evidence of estuary evolution: A rapid and
750 diagnostic tool for determining the nature of recent saltmarsh accretion.
751 Geomorphology, 213, 139-152.
752 Reichsamt für Landesaufnahme, 1943. Topographische Karte 1:25,000, Blatt:1618, Garding.
753 Reineck H.-E., Singh I.B., 1975. Depositional sedimentary environments. Springer, Berlin,
754 439 pp.
755 Schelling, H., 1952. Die Sturmfluten an der Westküste von Schleswig-Holstein. Die Küste, 1,
756 63-146.
757 Schlitzer, R., 2014. Ocean Data View. http://odv.awi.de.
758 Schuerch, M., Rapaglia, J., Liebetrau, V., Vafeidis, A., Reise, K., 2012. Salt marsh accretion
759 and storm tide variation: an example from a barrier island in the North Sea. Estuaries
760 and Coasts, 35, 486-500.

761 Schuerch, M., Vafeidis, A., Slawig, T., Temmerman, S., 2013. Modeling the influence of
762 changing storm patterns on the ability of a salt marsh to keep pace with sea level rise.
763 Journal of Geophysical Research: Earth Surface, 118, 84-96.
764 Schuerch, M., Dolch, T., Reise, K., Vafeidis, A.T., 2014. Unravelling interactions between salt
765 marsh evolution and sedimentary processes in the Wadden Sea (southeastern North
766 Sea). Progress in Physical Geography, 38, 691-715.
767 Schuerch, M., Spencer, T., Temmerman, S., Kirwan, M. L., Wolff, C., Lincke, D., McOwen,
768 C.J., Pickering, M.D., Reef, R., Vafeidis, A.T., Hinkel, J., Nicholls, R.J., Brown, S.,
769 2018. Future response of global coastal wetlands to sea-level rise. Nature, 561, 231-
770 234.
771 Scott, D.S., Medioli, F.S., 1978. Vertical zonations of marsh for- aminifera as accurate
772 indicators of former sea-levels. Nature, 272, 528-531.
773 Scott, D.S., Medioli, F.S., 1980. Quantitative studies of marsh foraminiferal distributions in
774 Nova Scotia: implications for sea level studies. Cushman Foundation for Foraminiferal
775 Research, Special Publication, 17, 58 pp.
776 Scott, D.B., Hermelin, J.O.R., 1993. A device for precision splitting of micropaleontological
777 samples in liquid suspension. Journal of Paleontology, 67, 151-154.
778 Scott, D.B., Collins, E.S., Gayes, P.T., Wright, E., 2003. Records of prehistoric hurricanes on
779 the South Carolina coast based on micropaleontological and sedimentological
780 evidence, with comparison to other Atlantic Coast records. Geological Society of
781 America Bulletin, 115, 1027-1039.
782 Stock, M., 2011. Patterns in surface-elevation change across a temperate salt marsh
783 platform in relation to sea-level rise. Coastline Reports, 17, 33-48.
784 Stock, M., Gettner, S., Hagge, H., Heinzel, K., Kohlus, J., Stumpe, H., 2005. Salzwiesen an
785 der Westküste von Schleswig-Holstein 1988–2001: Schriftenreihe des Nationalparks
786 Schleswig-Holsteinisches Wattenmeer, 240 pp.

787 Tomczak, G., 1952. Der Einfluß der Küstengestalt und des vorgelagerten Meeresbodens auf
788 den windbedingten Anstau des Wassers, betrachtet am Beispiel der Westküste
789 Schleswig-Holsteins. Deutsche Hydrographische Zeitschrift, 5, 115-132.
790 Turner, R.E., Baustian, J.J., Swenson, E.M., Spicer, J.S., 2006. Wetland sedimentation from
791 Hurricanes Katrina and Rita. Science, 314, 449-452.
792 Zitscher, F.-F., Scherenberg, R., Carow, U., 1979. Die Sturmflut vom 3. und 21. Januar 1976
793 an den Küsten Schleswig-Holsteins. Die Küste, 33, 71-100.
794
795

Supplement

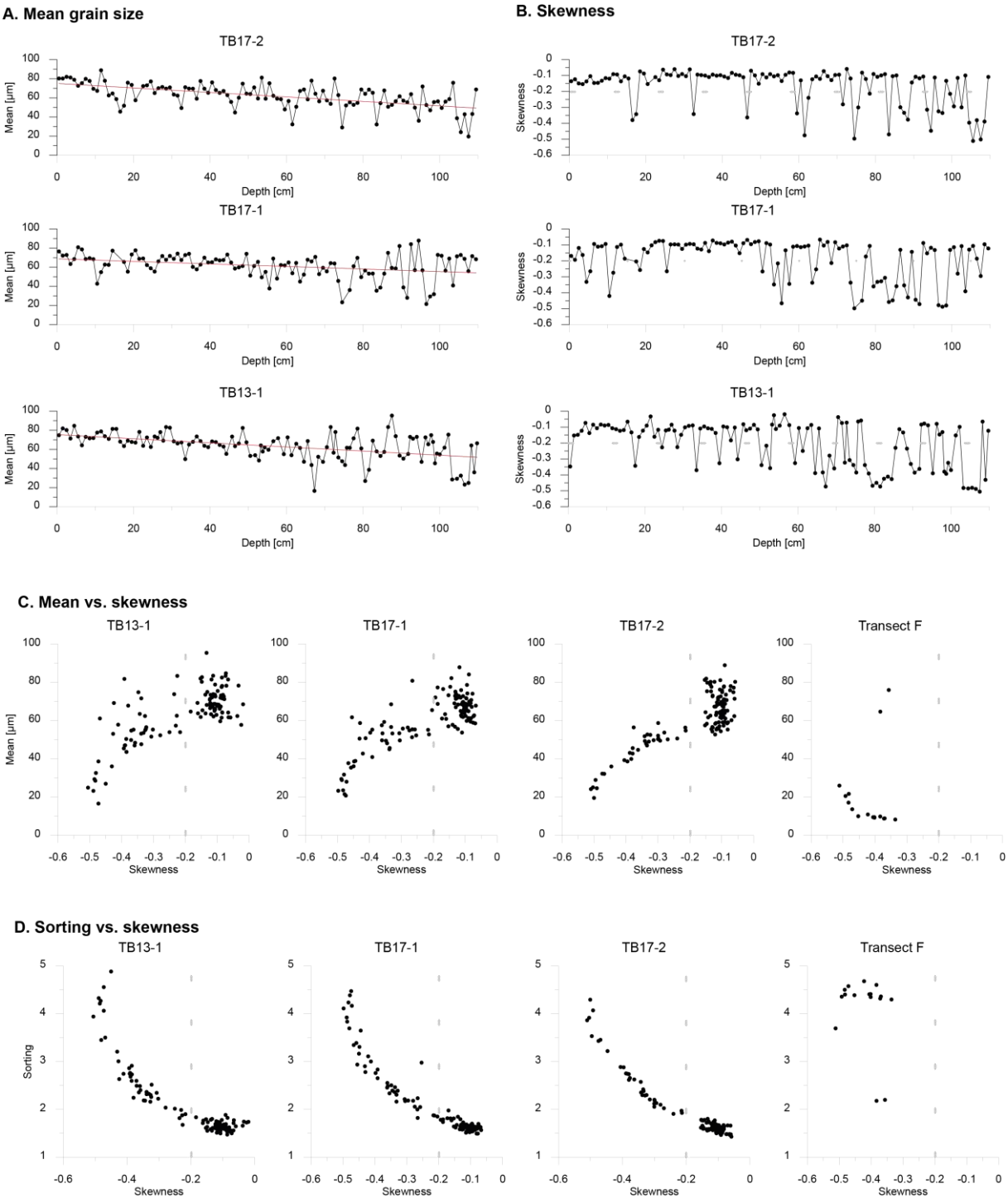

Supplement Figure 1: Mean grain size (A) and skewness of the grain-size distribution (B) of sediment sections TB13-1, TB17-1 and TB17-2. Mean grain-size versus skewness (C), and sorting versus skewness for sections TB13-1, TB17-1 and TB17-2, and surface transect F.